

# The Parallax and Proper Motion of RX J1856.5–3754 Revisited

D. L. Kaplan

*Department of Astronomy, 105-24 California Institute of Technology, Pasadena, CA 91125, USA*

`dlk@astro.caltech.edu`

M. H. van Kerkwijk

*Sterrenkundig Instituut, Universiteit Utrecht, Postbus 80000, 3508 TA Utrecht, The Netherlands*

`M.H.vanKerkwijk@phys.uu.nl`

and

J. Anderson

*Astronomy Department, University of California, Berkeley, CA 94720-3411, USA*

`jay@astron.berkeley.edu`

## ABSTRACT

RX J1856.5–3754, a bright soft X-ray source believed to be the nearest thermally emitting neutron star, has commanded and continues to command intense interest from X-ray missions. One of the main goals is to determine the radius of this neutron star. An integral part of the determination is an accurate parallax. Walter (2001) analyzed *Hubble Space Telescope (HST)* data and derived a parallax,  $\pi = 16.5 \pm 2.3$  mas. Combining this distance with the angular radius derived from blackbody fits to observations of RX J1856.5–3754 with *ROSAT*, *EUVE*, *HST*, Pons et al. (2001) derived an observed radius (“radiation radius”),  $R_\infty = 7$  km. This value is smaller than the radii calculated from all proposed equations-of-state (EOS) of dense baryonic matter (Haensel 2001). Here, we have analyzed the same *HST* data and find  $\pi = 7 \pm 2$  mas. We have verified our result using a number of different, independent techniques, and find the result to be robust. Adopting our parallax, the radius of RX J1856.5–3754 is  $R_\infty = 15 \pm 6$  km. This radius falls squarely in the range of radii, 12–16 km, expected from calculations of neutron star structure for different equations of state. With additional *HST* observations, the parallax estimate can be improved to the point by which the inferred radius can constrain the choice of EOS.

## 1. Introduction

The *ROSAT* all-sky survey identified six neutron stars that are radio-quiet but bright in the soft X-ray band. These sources, unlike the well studied radio pulsars, lack significant non-thermal emission and are thus excellent candidates for X-ray spectroscopic studies of the atmospheres of neutron stars (for reviews, see Motch 2000; Treves et al. 2000).

The brightest of these sources is RX J1856.5–3754 (Walter, Wolk, & Neuhäuser 1996). A faint, blue optical counterpart was identified from *Hubble Space Telescope (HST)* data (Walter & Matthews 1997). RX J1856.5–3754 has been intensively studied by most major facilities, especially *ROSAT*, *EUVE*, *ASCA* and *HST*. The broad-band data can be well fitted by thermal emission from a neutron star, which has resulted in the determination of the effective temperature,  $T_{\text{eff}}$ , and angular radius of the neutron star,  $R_{\infty}/d$  (Pons et al. 2001).

Walter (2001, hereafter W01) used *HST* data spanning three years to measure the astrometric parameters of RX J1856.5–3754, finding a parallax of  $16.5 \pm 2.3$  mas and a proper motion of  $332 \pm 1$  mas  $\text{yr}^{-1}$  at a position angle of  $100.3^{\circ} \pm 0.1^{\circ}$  ( $\mu_{\alpha} = 326.7 \pm 0.8$  mas  $\text{yr}^{-1}$ ,  $\mu_{\delta} = -59.1 \pm 0.7$  mas  $\text{yr}^{-1}$ ).

Combining this parallax with the broad-band modeling yields a radiation radius of  $\approx 7$  km. This radius is smaller than the Schwarzschild radius for the canonical mass of a neutron star,  $1.4 M_{\odot}$ . For the radius to exceed the Schwarzschild radius, the mass has to be less than  $1 M_{\odot}$  (Pons et al. 2001).

The importance of RX J1856.5–3754 as a laboratory for dense matter physics has motivated deep observations by *Chandra* (Burwitz et al. 2001), *XMM* and the Very Large Telescope (VLT). Results from the first 50-ksec *Chandra* observations<sup>1</sup> can be found in Burwitz et al. (2001); the blackbody fits are similar to those of Pons et al. (2001). Using the VLT, van Kerkwijk & Kulkarni (2001) discovered an unusual H $\alpha$  nebula around RX J1856.5–3754, from which they infer properties of RX J1856.5–3754’s energetics and emission characteristics (van Kerkwijk & Kulkarni 2001).

Parallax or distance is essential to obtaining the radius, the key physical parameter (since it now appears that the X-ray observations yield reliable values for  $T_{\text{eff}}$  and the angular radius). In view of the perplexing radius inferred from the parallax measurement of W01 we undertook an analysis of the publicly available *HST* data. Here we present a detailed description of our analysis followed by our measurement of the parallax.

---

<sup>1</sup>In early October, 2001, *Chandra* observed RX J1856.5–3754 for an additional 450-ksec under the aegis of the Director’s discretionary program.

## 2. Observations, Analysis & Results

We analyzed the publicly *HST*/WFPC2 observations described by W01 and Walter & Matthews (1997); see Table 1 for a log of the observations. As noted by W01, the observations took place near the times of parallactic maximum (3 October and 30 March). RX J1856.5–3754 is always on the Planetary Camera (PC) detector so we only analyzed those data.

### 2.1. Relative Astrometry

We used the effective point-spread function (ePSF) fitting technique to perform the astrometry, as described by Anderson & King (2000, hereafter AK00). We did not have sufficient numbers of stars to derive our own ePSF for each data set, so we used a previously determined ePSF (from archival data) for the *HST*/WFPC2 F555W filter. While the parallax data were taken with the F606W filter, we feel that using the F555W ePSF was appropriate, as it was of superior quality to the F606W ePSF that we have (also derived from other data). The difference in ePSFs should not bias the data, as the wavelength dependence of the ePSF is not strong, especially across the  $\approx 50$  nm difference in effective wavelength between the filters. Furthermore, the blue color of RX J1856.5–3754 brings its ePSF closer to the F555W ePSFs of normal stars. In any case, we also performed the analysis with the F606W ePSF. These ePSFs were not as of high quality as the F555W ePSF (owing to a less ideal data set), giving larger errors, but the results were entirely consistent with those obtained using the F555W ePSF.

We fit the F555W ePSF to the raw images, uncorrected for dithering or cosmic rays. For each epoch, we used a  $\chi^2$ -minimization, as described by AK00, to derive a position for each star in each of the raw images. We corrected this position for the 34th-row anomaly<sup>2</sup> (Anderson & King 1999) and geometric distortions in the PC detector using new coefficients (Anderson 2002, in preparation). For each epoch, this yielded four (or eight) positions for each star.

We then solved for the shifts (due to dithering) between the four (or eight) images in a given epoch. We rejected sources which had significantly higher residuals than other sources of their magnitude (see Figure 1), ascribable to the source being extended or saturated. For the remaining sources we used an iterative  $\sigma$ -clipping (with threshold at  $2.5\sigma$ ) to reject outlier position determinations. Following this the remaining position measurements were used to derive the average position for each source. The final distortion-corrected source positions in image  $(x, y)$  coordinates as well as the number of accepted measurements are listed in Table 3.

In the limit of a large number of independent observations that are well dithered, the measured

---

<sup>2</sup>It is a common error to apply the 34th-row correction *after* shifting and combining the data. This procedure is incorrect, as the 34th-row correction should be applied to the raw image coordinates and not those that have been shifted and rebinned.

rms would have yielded reliable uncertainties. However, we are limited by the available meager number of frames at each epoch. With a maximum of four (or even eight) measurements of each position we were not able to search for systematic errors. Furthermore, the data were taken with non-optimal dithering<sup>3</sup>. So we adopted a semi-empirical approach along the following lines. As the first approximation of the uncertainty for each position, we take the rms variation between the positions used to construct the average.

As the next level in our analysis, we used the expected precision in the positions as a function of the signal-to-noise ratio (SNR) of stars to estimate uncertainties in our positions. To this end, we utilized an astrometric database that one of us (J.A.) has built up over the last several years. In particular, we used 18 well-dithered PC images that were obtained under similar conditions (filter, background, crowding) to those discussed here. In Figure 1 we display a fit (obtained from the measurements of about 5000 stars) to the astrometric precision as a function of the SNR of stars. The relation from Figure 1 is reasonably well fit by

$$\sigma = \frac{1}{\sqrt{2}} \left[ (2.38e^{0.69m})^3 + (0.02)^3 \right]^{1/3} \text{ pixels}, \quad (1)$$

where  $m = -2.5 \log_{10}(\text{DN})$  (within a  $5 \times 5$  pixel area) is the magnitude measured in a single exposure and  $\sigma$  is the 1-D position uncertainty. For  $N$  well-dithered exposures, the uncertainty is  $\sigma/\sqrt{N}$ , as expected (AK00).

We see that the raw uncertainties generally follow the expected trend, but that there is substantial variation. This is not surprising, given that we may be computing the uncertainties from four or fewer than four measurements. Therefore, in our analysis we use the maximum of the empirically determined uncertainty for an individual star and the uncertainty from the relation in Figure 1 corrected to the appropriate magnitude; the stars that have uncertainties larger than those inferred from this relation do so due to cosmic rays or proximity to bright sources.

The above analysis gives us reliable and accurate measurements of stellar positions, but while these stars are in the background relative to RX J1856.5–3754 they can still have their own motions that will bias our determinations. Therefore, to have some idea of the absolute motion of the stars in the image, we included in the data measurements of the positions of two slightly extended sources (presumed to be galaxies) present on the *HST* images (see Table 2). As these sources are non-stellar, we could not use the AK00 technique to measure their positions. Instead we fitted Gaussian profiles and then applied the same distortion corrections as with the other technique. Gaussian fitting is inherently less accurate than ePSF fitting (AK00), but the errors are important primarily for sources that are undersampled by the WFPC2 pixels (i.e. where pixel-phase errors are important). The galaxies were reasonably well resolved ( $\text{FWHM} \approx 3.2$  pixels for source #20,  $\text{FWHM} \approx 3.6$  pixels for source #104), so they should not suffer from systematic errors relating to undersampling.

---

<sup>3</sup>For astrometric purposes, a  $2 \times 2$  dithering grid is minimal for optimal removal of pixel-phase errors; a 15-point dither pattern is even better. See AK00.

## 2.2. Registration of Epochs

To determine the transformation of the background sources (all sources except for RX J1856.5–3754) between epochs, we proceeded iteratively. Our basic input data set was the 27 stellar sources that had consistent measurements in each epoch plus the two galaxies (Section 2.1), given in Table 3. The faintest of these sources were as faint as RX J1856.5–3754, and the brightest were  $\approx 160$  times as bright as RX J1856.5–3754 (the brightest non-saturated sources on the WFPC2 images). First, we set the fiducial positions of the sources to their measured positions at epoch 1999.7. We chose this epoch as the effects of parallax between it and epoch 1996.8 are minimized (due to similar parallactic angles) and the effects of proper motion between it and epoch 1999.3 are minimized (due to close proximity in time), thus yielding the best matches to the other epochs given the limited information that we have. We assumed that the position angle, scale, and pointing center of this fiducial epoch are known. The pointing center has no impact on the results, and is simply a dummy parameter. The position angle and scale are known to reasonable precision ( $< 0.1^\circ$  for the position angle, and  $< 0.1\%$  for the scale). For our nominal values, we take the values from the *HST* image headers (listed in Tables 1). If these values are wrong at certain levels, they would introduce errors on those levels into our measurements (i.e. if the fiducial scale were wrong by 0.1%, our proper motions would be wrong by the same amount) but these are systematic effects that are well below the measurement precision of the current data.

For our transformation between the epochs, we assumed a simple rotation, scale, and offset. This is valid if the distortion correction (Section 2.1) removed all nonlinear terms. The transformation equation between the measured positions of star  $i$  at epoch  $j$ ,  $(x_{i,j}, y_{i,j})$ , to the celestial position  $(\Delta\alpha_{i,j}, \Delta\delta_{i,j})$  is

$$\begin{aligned}\Delta\alpha_{i,j} &= -\text{scale}_j ((x_{i,j} - x_{0,j}) \cos \text{PA}_j - (y_{i,j} - y_{0,j}) \sin \text{PA}_j) \\ \Delta\delta_{i,j} &= \text{scale}_j ((x_{i,j} - x_{0,j}) \sin \text{PA}_j + (y_{i,j} - y_{0,j}) \cos \text{PA}_j),\end{aligned}\quad (2)$$

where  $\text{scale}_j$  is the plate scale (arcsec per pixel),  $(x_{0,j}, y_{0,j})$  are the offsets, and  $\text{PA}_j$  is the position angle of epoch  $j$ , all of which are given in Table 1.

We performed a  $\chi^2$  fit between the fiducial positions and the positions at the three measured epochs, varying the scale, position angle, and offsets of the other epochs. This fit gave relatively large  $\chi^2$  values, due to proper motion between the epochs.

We then fit for updated fiducial positions and proper motions of the background sources based on a linear least-squares technique (for the galaxies, the proper motion was forced to be 0). These positions and proper motions were used to re-calculate the expected positions in the non-reference epochs, which dramatically lowered the  $\chi^2$  values. We iterated this procedure (fitting for the transformation between the epochs, then fitting for the individual positions and proper motions) making sure that the solution was converging. After five iterations,  $\chi^2$  changed by 0.2;

we considered the solution to have converged. The results of the fitting (the fiducial positions and proper motions) are given in Table 2.

We did not fit for the parallaxes of the background sources as they are all at distances of  $> 1$  kpc (see Appendices A and B). Our final  $\chi^2$  value for the fit was 251 for 48 degrees of freedom. The implied reduced  $\chi^2$  deviates significantly from 1, indicating that we are missing some source of error in our analysis. Therefore we performed additional analyses to determine how robust our measurements are, and included information from these analyses in the final estimates (see Section 2.4 and Appendix A).

The deviations of the scales and position angles from the nominal value were small but significant (see Table 1), unlike stated by W01. We find that the scale changed by  $\approx 0.03\%$  from one epoch to another, and that the position angle changed by  $\approx 0^\circ.02$ . This is reasonable, given the fluctuations seen in other WFPC2 observations (due to thermal fluctuations in the detector and telescope assembly; AK00).

### 2.3. Absolute Astrometry

Absolute astrometry was done relative to the USNO-A2.0 catalog (Monet 1998). We first determined centroids for 581 USNO-A2.0 stars that overlapped with an average B-band image obtained in 1999 using FORS1 on UT#1 (Antu) at the Very Large Telescope (see van Kerkwijk & Kulkarni 2001; the image is composed of three 5-minute exposures). We rejected 82 objects that were overexposed or had widths inconsistent with them being stellar. Next, the pixel coordinates were corrected for instrumental distortion using a cubic radial distortion function provided to us by T. Szeifert and W. Seifert (1999, private communication). Finally, the zero point position, the plate scale, and the position angle on the sky were determined, rejecting iteratively a further 90 objects for which the residuals to the solution were larger than  $0''.6$  (inspection of the images showed that virtually all of these were visual doubles, which are blended on the sky survey plates on which the USNO-A2.0 coordinates are based). For the 409 stars that pass our cuts, the inferred single-star measurement errors are  $0''.19$  in each coordinate, which is line with the uncertainties expected for the USNO-A2.0 catalogue (Deutsch 1999). Thus, we conclude that our astrometry is tied to the USNO-A2.0 system at about  $0''.01$  accuracy.

The solution was transferred to the October 1999 F606W *HST* frames using 13 transfer stars, solving only for zero point offset (i.e., using the scale and orientation listed in the header). Some of the transfer stars were overexposed, but the positions still were reasonably accurate. With this solution, we determined the absolute positions listed in Table 2.

The solution was transferred to the March 1999 F606W *HST* frames using 13 transfer stars. Some of those were overexposed, but the centroids still were reasonably accurate. The measured PC pixel positions were corrected for instrumental distortion using the bi-cubic function given by Holtzman et al. (1995). The inferred single-star measurement errors are  $0''.016$  in each coordinate,

and the zero-point should thus be tied to the B image to within  $0''.005$ . With this solution, the positions of the other stars on the 1999 F606W image were calculated.

#### 2.4. Determination of Parallax and Proper Motion of RX J1856.5–3754

With the three epochs registered, we compared the positions of RX J1856.5–3754 in each (see Table 3). We combined the initial estimates of the position uncertainties in quadrature with the uncertainties introduced by the registration, but the registration uncertainties were relatively small. We fit for the proper motion and parallax of RX J1856.5–3754 using a linear least-squares solution. The locations along the parallactic ellipse at each epoch were determined using the prescription of the Astronomical Almanac (1999; p. C24).

As noted in Sections 2.1 and 2.2, our limited number of measurements means that the individual position uncertainties have limited accuracy. Therefore, the derived uncertainty on the parallax (1.7 mas) may not be correct. We have therefore estimated the parallax uncertainty using a variety of techniques (see Appendix A); these techniques have an rms of 0.4 mas, which we add in quadrature to find an rms of 1.8 mas. We round this up, finding the overall  $1-\sigma$  uncertainty to be 2 mas, similar to the value found by W01.

We present the results of the fitting for  $\pi$ ,  $\mu_\alpha$ , and  $\mu_\delta$  in Table 4. We also present the values for the derived parameters of distance  $D$  and transverse velocity  $V_\perp$ . The best-fit parallax is  $7 \pm 2$  mas. We can exclude a null-result for the parallax at the  $10^{-4}$  level. Our results are inconsistent with those of W01 at the 99.8% level. However, our best-fit values for the proper motions are entirely consistent with those presented in W01, and also agree with the orientation of the H $\alpha$  nebula (van Kerkwijk & Kulkarni 2001).

The severe inconsistency between the values of the parallax derived by W01 and that derived by us is puzzling. The most obvious explanation is the significant difference in the way the data were processed: we used an ePSF that accounts for pixel phase errors and fit the data without manipulations such as rebinning or resampling. We also use more accurate distortion corrections, account for small changes in the scale and position angle of the observations from their nominal values, and account for the proper motion of the background objects. W01, on the other hand, first resampled the data, then shifted, then rebinned the data, and measured the positions with a PSF that is independent of pixel phase. Such analysis is liable to introduce even more pixel phase errors than those that were originally present. However, even if we follow the general method of W01 (resampling and rebinning, Gaussian fitting, old distortion corrections) we cannot reproduce a parallax of 16.5 mas (see Appendix A).

The surest way to resolve the differences between our analysis and that of W01 will be with the 2001 March *HST* data (not yet publicly available). This should allow further refinement of the proper motion and a more robust measurement of the parallax, with a final uncertainty of  $\approx 1.5\text{--}2$  mas.

As noted by W01, due to the small angle between the proper motion and the major axis of the parallactic ellipse, there is significant anti-correlation between the parallax and the magnitude of the proper motion. This is shown in Figure 2. We stress, though, that even with the latitude given by this anti-correlation we cannot accommodate a parallax of 16.5 mas.

The position offsets with the proper motion subtracted are shown in Figure 3. The offsets are consistent with the best-fit parallax. The correlation between motion due to parallax and due to proper motion is also illustrated in Figure 3 — the proper motion direction differs from the position angle of the parallactic ellipse by only  $20^\circ$ .

### 3. Discussion

#### 3.1. Mass & Radius

The most immediate impact of a revised distance for RX J1856.5–3754 is in the interpretation of its spectrum. Pons et al. (2001) used spectral fits to X-ray and broad-band data to determine a best-fit mass and radius, taking the previously published distance of  $d = 61$  pc (W01) to convert the measured angular size  $R_\infty/d$  to a radius  $R_\infty$ , where  $R_\infty$  is the “radiation” radius determined from blackbody fitting. The best-fit radius for all atmosphere choices was  $R_\infty = 6$  km; causality then requires that the mass be less than this (in geometric units), giving  $M < 1M_\odot$  (Haensel 2001). These values are inconsistent with all neutron star equations-of-state (EOS), most of which have radii  $R \geq 10$  km (Thorsett & Chakrabarty 1999; Lattimer & Prakash 2000).

Our new distance pushes RX J1856.5–3754 further away, and therefore allows for larger radii and masses. For example, the best-fit uniform temperature blackbody fit (a uniform temperature is almost required by the limits on pulsations; Burwitz et al. 2001) has  $R_\infty/d = 0.11 \pm 0.01$  km pc $^{-1}$  (Pons et al. 2001), which had implied  $R_\infty \approx 6.7$  km for a distance of 61 pc. Using our revised parallax value changes the radius to  $R_\infty \approx 15$  km, giving a physical radius of  $R \approx 12$  km (for the canonical neutron star mass of  $1.4M_\odot$ ; Thorsett & Chakrabarty 1999). This is much more in line with the likely values for  $R$  determined by equations of state (e.g., Lattimer & Prakash 2000).

Paczyński (2001) has predicted that the passage of RX J1856.5–3754 near star 115 (from W01) in 2003 will cause the apparent position of star 115 to change by  $\approx 0.6$  mas due to gravitational lensing<sup>4</sup>. Paczyński (2001) goes on to suggest that precise measurement of this deflection, perhaps by the new Advanced Camera for Surveys (ACS) aboard *HST*, could be used to measure the mass of RX J1856.5–3754 and provide an independent estimate to constrain the equation of state. Unfortunately, based on the current WFPC2 data, it appears impossible to measure (in a reasonable number of orbits) the position of the star with enough precision to perform the suggested measurements, even with the ACS.

---

<sup>4</sup>We do note include star 115 in our analysis because it is fainter than our detection threshold.

### 3.2. Energetics and Origin

Another area where the distance enters is in modeling of the H $\alpha$  nebula that surrounds RX J1856.5–3754 (van Kerkwijk & Kulkarni 2001). In most of the modeling, the distance enters linearly and the factor of  $\sim 2$  difference that we find here will not significantly change the conclusions. However, there are a number of quantities that have steep dependencies on the distance. We examine each of these.

In their estimate of the minimum pulsar wind energy loss  $\dot{E}$  in the bow-shock model, van Kerkwijk & Kulkarni (2001) find that  $\dot{E} \propto d^3$ . We are able therefore to revise the limit to  $\dot{E} \gtrsim 8 \times 10^{32} d_{140}^3 \text{ erg s}^{-1}$ , where the distance to RX J1856.5–3754 is  $140d_{140}$  pc. This then impacts on the estimates of the inferred spin period  $P$  and magnetic field  $B$ , giving  $P \lesssim 12$  s and  $B \lesssim 5 \times 10^{13}$  G.

If RX J1856.5–3754 were powered by accretion, van Kerkwijk & Kulkarni (2001) find an accretion rate  $\dot{M} = 3 \times 10^9 d_{60}^{-3.5} \text{ g s}^{-1}$ , where the distance  $d = 60d_{60}$  pc. For  $d_{60} = 2.3$ , as we find here, this then implies an available accretion power of  $\sim 3 \times 10^{28} \text{ g s}^{-1}$ . This is now almost four orders of magnitude less than the observed bolometric luminosity of RX J1856.5–3754, which is revised upwards to  $\sim 2 \times 10^{32} d_{140}^2 \text{ erg s}^{-1}$ , further supporting the claim that accretion cannot power the source.

The final model for the H $\alpha$  nebula considered by van Kerkwijk & Kulkarni (2001) is an ionization nebula. Here, RX J1856.5–3754 can still be a pulsar, but its energy loss  $\dot{E}$  must be small enough that any bow-shock nebula is smaller than the observed nebula. This leads to the result  $\dot{E} \lesssim 2 \times 10^{34} d_{140}^{3.5} \text{ erg s}^{-1}$ , a much less constraining value than that given in van Kerkwijk & Kulkarni (2001).

### 3.3. Local Density of Neutron Stars

Once the emission characteristics and size of one neutron star are well determined, they can be used to calibrate other sources. As an example, we derive a relation between the optical magnitude, X-ray blackbody temperature, and distance for isolated neutron stars, and apply it to the two brightest isolated neutron stars and PSR B0656+14, a nearby radio pulsar.

The optical emission from RX J1856.5–3754 and another isolated neutron star, RX J0720.4–3125 (Haberl et al. 1997; Kulkarni & van Kerkwijk 1998), is very well described by the Rayleigh-Jeans tail of a blackbody, although at a level slightly above that inferred from blackbody fits to the X-ray data (van Kerkwijk & Kulkarni 2001). In particular,  $f_\nu \propto \nu^2$  in the optical regime. If we assume that the surface compositions of isolated neutron stars are similar, then  $f_\nu \propto R^2 kT \nu^2 / d^2$ , where  $R$  is the neutron star radius,  $kT$  is the effective temperature of the surface, and  $d$  is the distance. If the neutron stars all have the same radii, we can write

$$d_{100} = 1.4 \sqrt{\frac{kT}{57 \text{ eV}}} 10^{(V-25.7) \text{ mag/5}} = 1.4 \sqrt{\frac{kT}{57 \text{ eV}}} 10^{(B-25.3) \text{ mag/5}}, \quad (3)$$

where  $d = 100d_{100}$  pc, and  $B$  and  $V$  are the observed optical magnitudes. Here we use the best-fit blackbody temperature; while this is not always the best-fit overall to the X-ray emission (Pons et al. 2001), it is a simple model and the dependence of  $d_{100}$  on  $kT$  is rather weak, so it suffices. We list the implied distances for the three other neutron stars that have thermally-dominated X-ray emission and optical counterparts in Table 5. As a general result of our new parallax, we decrease the local density of isolated neutron stars by a factor of  $\sim 10$  with respect to that inferred from W01.

For the radio pulsar B0656+14 we get a distance of  $d_{100} \approx 3.3$ , near the low end of the values estimated through other means (250–800 pc; Mignani, De Luca, & Caraveo 2000) but still plausible. We understand that W. Brisken will soon have a VLBA measurement of the parallax, which should provide independent confirmation of our results (W. Brisken 2001, personal communication).

Data are based on observations with the NASA/ESA Hubble Space Telescope, obtained from the data Archive at the Space Telescope Science Institute, which is operated by the Association of Universities for Research in Astronomy, Inc., under NASA contract NAS 5-26555. D.L.K. holds a fellowship from the Fannie and John Hertz Foundation, and his research is supported by NSF and NASA. M.H.v.K. is supported by a fellowship from the Royal Netherlands Academy of Arts and Sciences. We thank S. Kulkarni and D. Frail for valuable discussions.

## A. Details of Analysis

To test the robustness of our analysis, we performed the same general analysis but with variations on the input data set and analysis method. These variations included combinations of:

- Using a six-parameter linear transformation between the epochs (instead of the standard four-parameter transformation involving a shift, scale, and rotation).
- Rejecting the stars with the largest position uncertainties.
- Rejecting the stars whose derived proper motions had the largest uncertainties.
- Rejecting the stars more than 300 pixels ( $15''$ ) from RX J1856.5–3754.
- Rejecting up to 10 stars at random from the sample.
- Using the F606W ePSF instead of the F555W ePSF (see Section 2.1)

All of these analyses gave entirely consistent results with rms variance of 0.4 mas, showing that our parallax measurements are not biased by any particular data points. Comparison of these parallax determinations allows us to better estimate the uncertainty in the parallax. To the formal error

determined from the least-squares fit (1.7 mas), we add (in quadrature) the 0.4 mas rms found above.

As another test, we used the same algorithm to measure the parallaxes of all of the other stellar sources in the *HST* images. As expected from their photometric distances (Appendix B), there were no convincing parallax measurements for these sources. The measured parallaxes had a mean of  $-0.3$  mas and a variance of 1.2 mas. The variance in the measured parallax was roughly independent of the brightness of the star, down to the brightness of RX J1856.5–3754, and is reasonably consistent with our estimation of the uncertainty of the parallax of RX J1856.5–3754. We therefore believe that a conservative estimate of the  $1\sigma$  parallax uncertainty to be 2 mas.

Finally, we performed the same analysis but with the initial astrometry done using more conventional Gaussian fitting and with older WFPC2 distortion coefficients (Holtzman et al. 1995; Trauger et al. 1995), like W01. Again, the results were consistent with those found using the more accurate ePSF fitting.

## B. Background Sources

Figure 4 shows the color-magnitude diagram for the background sources that have reliable VLT photometry (van Kerkwijk & Kulkarni 2001; van Kerkwijk & Kulkarni 2001) and the distances implied from main-sequence fitting. Almost all of the sources are bounded by main sequences with distances from 2–25 kpc, with a number at implied distances of 10–15 kpc. Alternately, a number of the sources are consistent with red-giant branch stars at a distance  $\sim 25$  kpc.

The implied distances of some of these sources, up to 25 kpc, places them at the edge of the Milky Way and  $\approx 2.5$  kpc above the disk, making them unlikely to be part of the Milky Way. The sources may be, however, in the Sgr dwarf galaxy. The heliocentric distance of the Sgr dwarf galaxy is  $\approx 25$  kpc, and it has a line-of-sight extent of  $\lesssim 8$  kpc (Ibata et al. 1997). The region near RX J1856.5–3754 is  $\approx 7.5^\circ$  from the center of the Sgr dwarf galaxy (Ibata et al. 1997), plausibly within the solid angle subtended by the Sgr dwarf galaxy. Therefore a number of the stars in the field could be main-sequence or giant stars in the Sgr dwarf galaxy.

Regardless, all of the background sources for which we have reliable photometry are at distances  $> 1$  kpc, so it is reasonable to ignore their parallaxes in the analysis.

In Figure 5, we show the proper motion vectors for the background sources determined from the fitting. Most of the motions are small,  $< 5$  mas  $\text{yr}^{-1}$ , with the majority being  $\approx 2$  mas  $\text{yr}^{-1}$ . This is consistent with the magnitude of the proper motion of the Sgr dwarf galaxy,  $250$  km  $\text{s}^{-1}$  at a distance of 25 kpc. The two galaxies (which were forced to have zero proper motion in our analysis) provide an absolute reference for these proper motions. The net proper motion of the background sources is  $\lesssim 0.5$  mas  $\text{yr}^{-1}$ . As this is less than the uncertainty in the measured proper motion for RX J1856.5–3754, the motion of the background sources should not bias the parallax

of RX J1856.5–3754.

## REFERENCES

Anderson, J. & King, I. R. 1999, PASP, 111, 1095

—. 2000, PASP, 112, 1360

Burwitz, V., Zavlin, V. E., Neuhaüser, R., Predehl, P., Trümper, J., & Brinkman, A. C. 2001, A&A, in press (astro-ph/0109374)

Cox, A. N. 2000, *Allen's astrophysical quantities*, 4th edn. (AIP Press/Springer: New York)

Deutsch, E. W. 1999, AJ, 118, 1882

Haberl, F., Motch, C., Buckley, D. A. H., Zickgraf, F. J., & Pietsch, W. 1997, A&A, 326, 662

Haensel, P. 2001, A&A, submitted (astro-ph/0105485)

Holtzman, J. A., Hester, J. J., Casertano, S., Trauger, J. T., Watson, A. M., Ballester, G. E., Burrows, C. J., Clarke, J. T., et al. 1995, PASP, 107, 156

Ibata, R. A., Wyse, R. F. G., Gilmore, G., Irwin, M. J., & Suntzeff, N. B. 1997, AJ, 113, 634

Koptsevich, A. B., Pavlov, G. G., Zharikov, S. V., Sokolov, V. V., Shibanov, Y. A., & Kurt, V. G. 2001, A&A, 370, 1004

Kulkarni, S. R. & van Kerkwijk, M. H. 1998, ApJ, 507, L49

Lattimer, J. M. & Prakash, M. 2000, Phys. Rep., 333, 121

Mignani, R. P., De Luca, A., & Caraveo, P. A. 2000, ApJ, 543, 318

Monet, D. E. A. 1998, in *The PMM USNO-A2.0 Catalog* (U.S. Naval Observatory, Washington DC)

Motch, C. 2000, preprint (astro-ph/0008485)

Paczynski, B. 2001, astro-ph/0107443

Pavlov, G. G., Welty, A. D., & Córdova, F. A. 1997, ApJ, 489, L75

Pons, J. A., Walter, F. M., Lattimer, J. M., Prakash, M., Neuhaüser, R., & An, P. 2001, ApJ, submitted (astro-ph/0107404)

Schwöpe, A. D., Hasinger, G., Schwarz, R., Haberl, F., & Schmidt, M. 1999, A&A, 341, L51

Thorsett, S. E. & Chakrabarty, D. 1999, ApJ, 512, 288

Trauger, J. T., Vaughan, A. H., Evans, R. W., & Moody, D. C. 1995, in Calibrating Hubble Space Telescope. Post Servicing Mission. Proceedings of a Workshop held at the Space Telescope Science Institute, in Baltimore, Maryland, May 15-17, 1995. Editor(s), Anuradha Koratkar, Claus Leitherer; Publisher, Space Telescope Science Institute, Baltimore, Maryland, 1995. LC #: QB500.268 .C34 1995. ISBN #: NONE., p.379, 379

Treves, A., Turolla, R., Zane, S., & Colpi, M. 2000, PASP, 112, 297

U. S. Naval Observatory & Royal Greenwich Observatory. 1998, The Astronomical Almanac for the year 1999 (The Astronomical Almanac for the year 1999, Publisher: Washington: United States Government Printing Office (USGPO) and London: Her Majesty's Stationery Office (HMSO), 1998)

van Kerkwijk, M. H. & Kulkarni, S. R. 2001, A&A, 378, 986

van Kerkwijk, M. H. & Kulkarni, S. R. 2001, A&A, in press (astro-ph/0110065)

Walter, F. M. 2001, ApJ, 549, 443

Walter, F. M. & Matthews, L. D. 1997, Nature, 389, 358

Walter, F. M., Wolk, S. J., & Neuhäuser, R. 1996, Nature, 379, 233

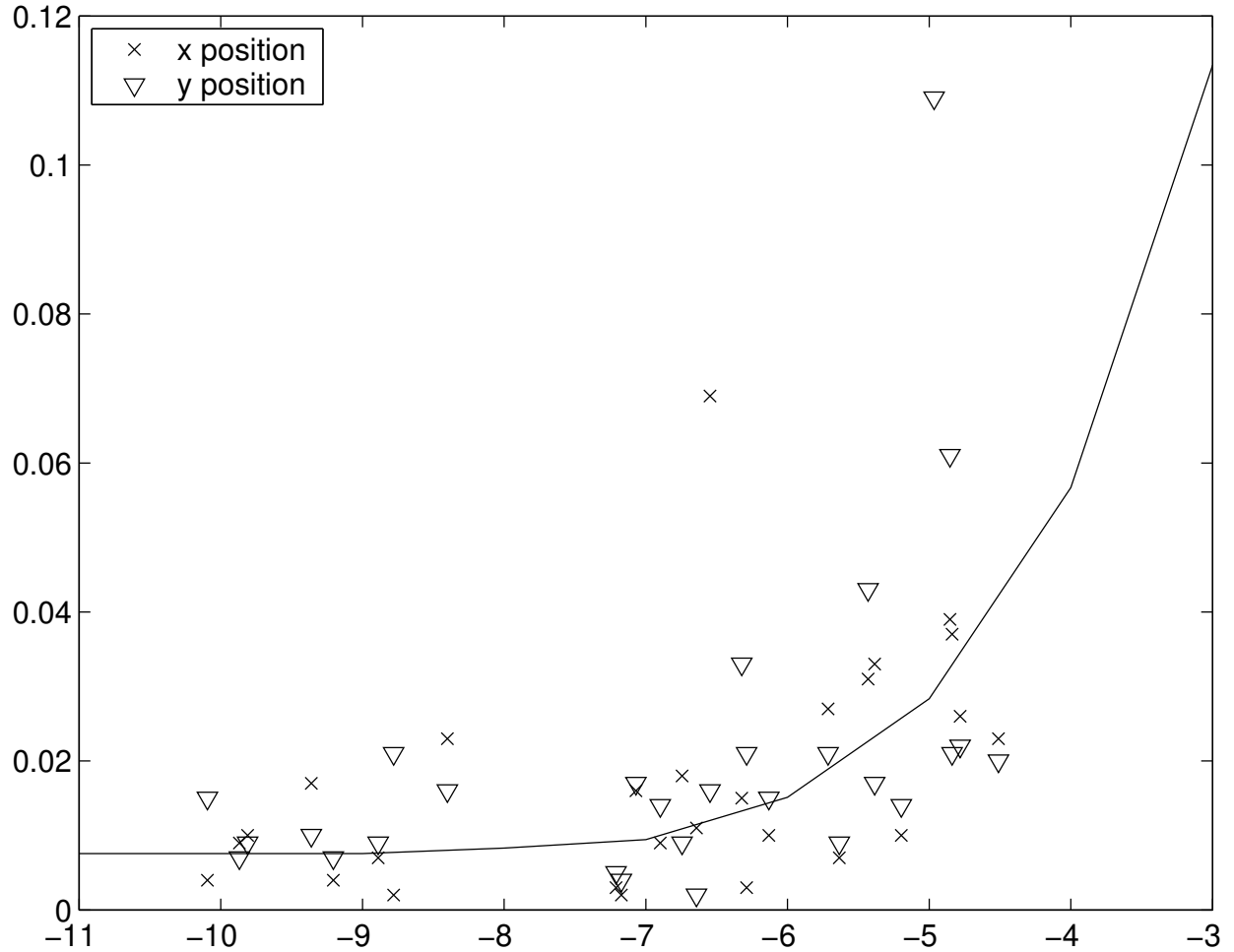


Fig. 1.— 1-D position uncertainty (pixels) vs. instrumental magnitude, defined by  $m = -2.5 \log_{10}(\text{DN})$  within a  $5 \times 5$  pixel region in a single exposure. The x's are for the raw uncertainties in the  $x$  positions of the stars used to register the different epochs, the triangles for the raw  $y$  uncertainties, and the solid line is a relation determined from  $\sim 5000$  well-observed stars in other data sets. The sources here are those that are not saturated and were used in the analysis; see Tables 2 and 3. The data from this paper (x's and triangles) generally follow the trend defined by the line (also given in Eqn. 1), but there is considerable spread due to the small number of measurements (3 or 4) used to construct each uncertainty.

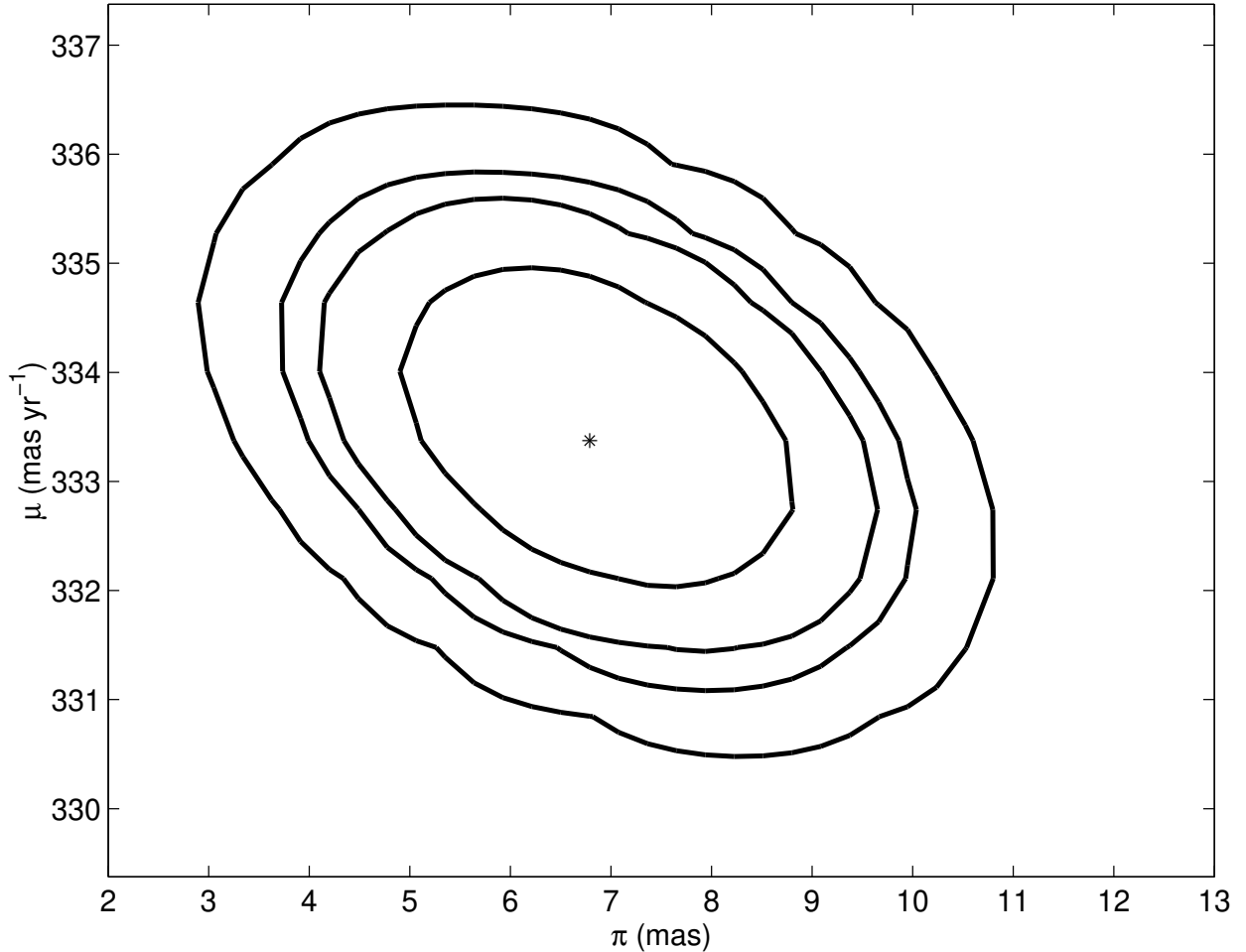


Fig. 2.— Joint confidence contours for the parallax  $\pi$  (mas) and the magnitude of the proper motion  $\mu$  (mas  $\text{yr}^{-1}$ ) for RX J1856.5–3754, illustrating the covariance between these parameters. Plotted are 68%, 90%, 95%, and 99% confidence contours, with the best-fit values indicated by the star. Note that the contours are for the joint confidence — the 1-D 68% confidence levels are given in Table 4. Compare to Fig. 2 from W01.

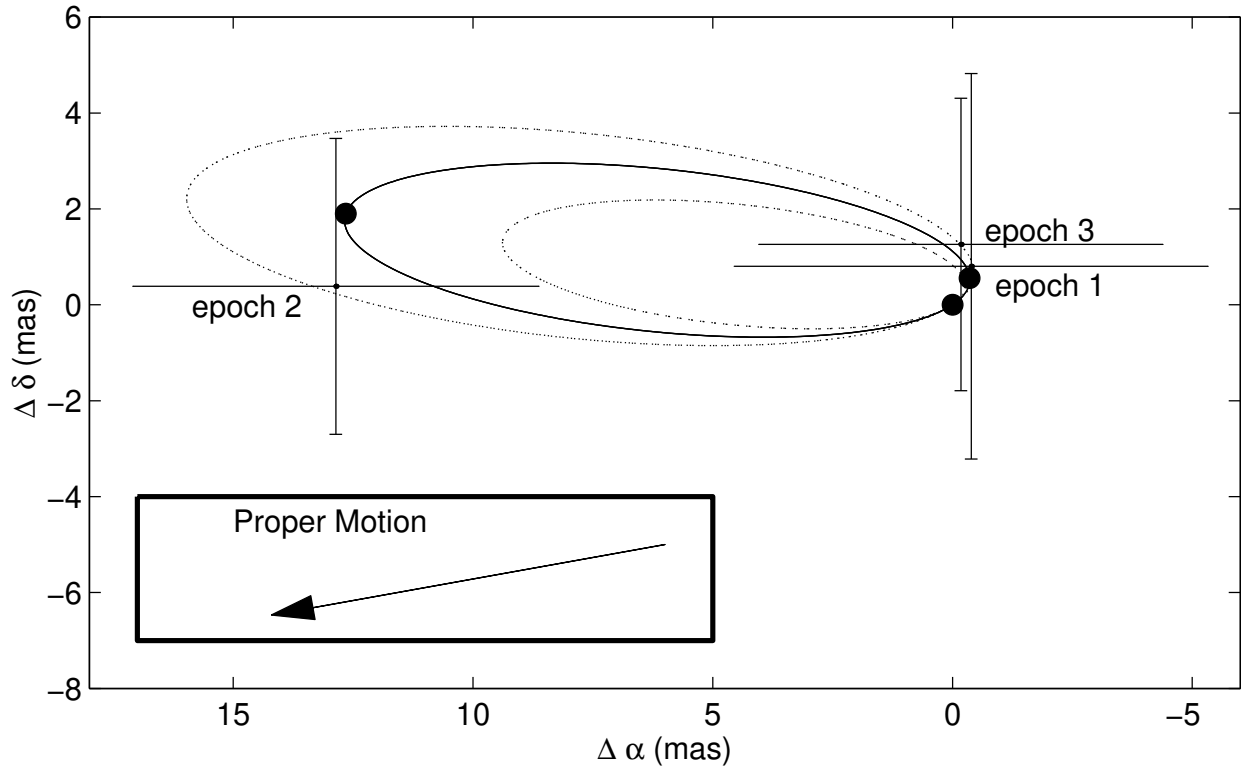


Fig. 3.— Parallactic ellipse for RX J1856.5–3754, showing the measured positions (points with error-bars) and expected positions (filled circles) at each epoch (after subtracting the best-fit proper motion). The inset shows an arrow that indicates the direction of the proper motion. The solid ellipse is for the best-fit parallax of 7 mas, while the dotted ellipses are for the  $\pm 1\sigma$  values of 5 and 9 mas. This figure can be compared to Fig. 4 from W01.

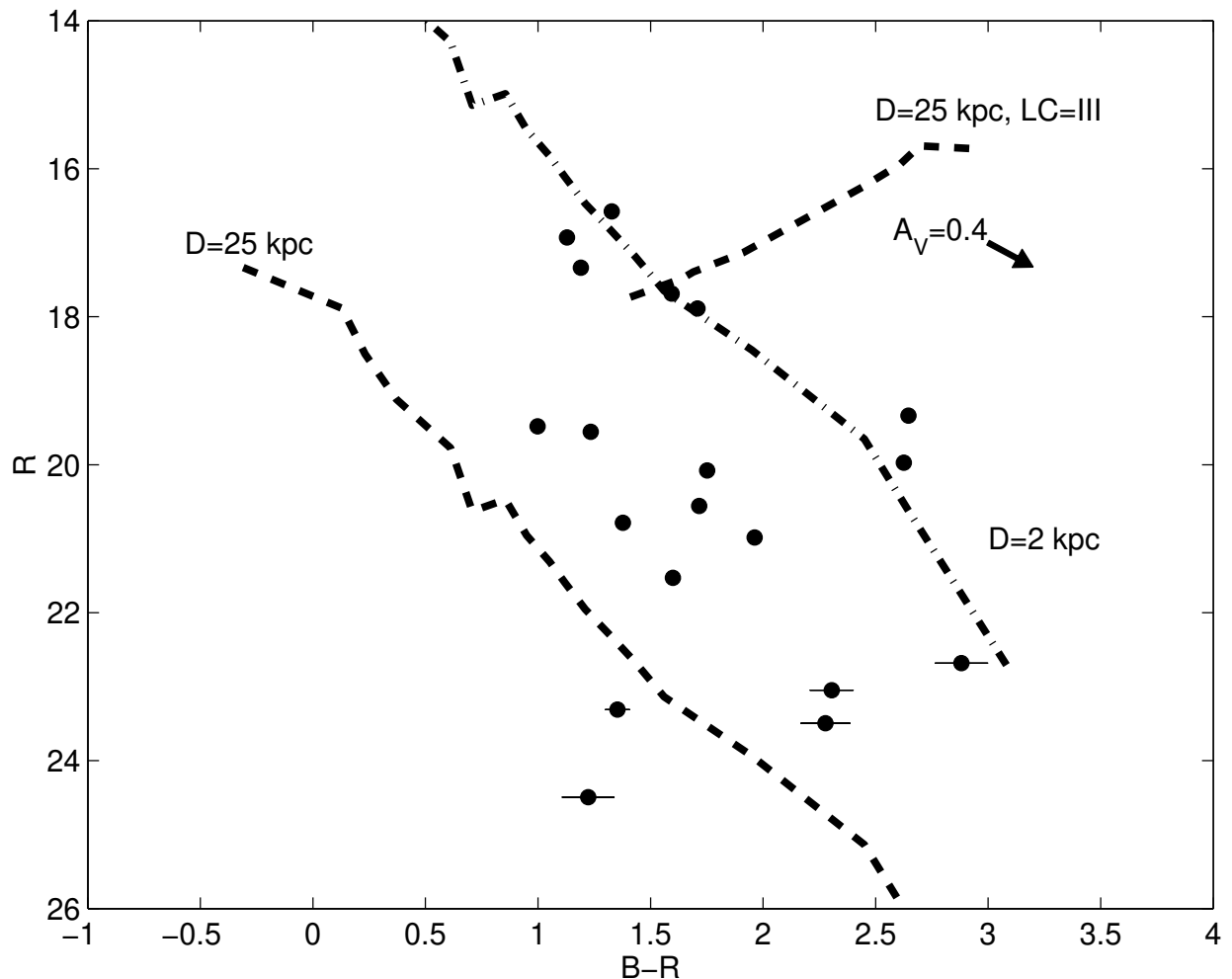


Fig. 4.— Color-magnitude diagram for background sources.  $R$  vs.  $B - R$ , with a  $A_V = 0.4$  mag reddening vector and a model main sequences at a distance of 2 kpc (dash-dotted line), a main sequence at a distance of 25 kpc (dotted line), and a giant branch at a distance of 25 kpc (dotted line, marked “LC=III”) from Cox (2000, p. 388, p. 392).

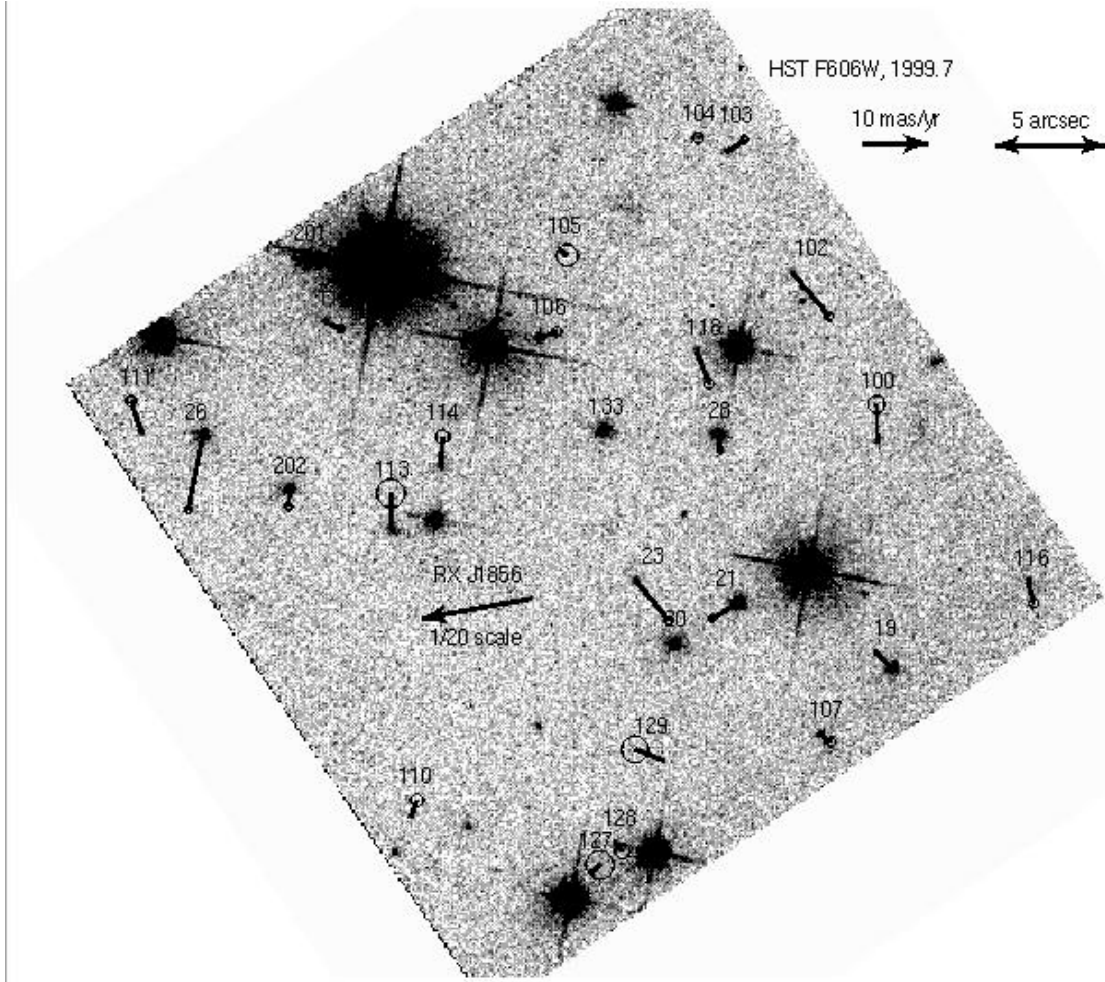


Fig. 5.— Derived proper motions for the background stars and galaxies used to register the three epochs, overlayed on the 1999.7 *HST* image. The lines indicate proper motions going from the stars to the circles. The sizes of the circles indicate the errors in the proper motions (scaled so that the reduced  $\chi^2$  is 1.0). The arrow in the upper right indicates proper motion with a magnitude of  $10 \text{ mas yr}^{-1}$ ; next to it is a  $5''$  scale bar. North is up, and East is to the left. The arrow from the position of RX J1856.5–3754 indicates the direction but only 1/20 the magnitude of the source’s proper motion (no uncertainties are plotted for RX J1856.5–3754 as its proper motion is scaled such that the uncertainties would be invisible). All sources are labeled with identifiers from Table 2.

Table 1. WFPC2 Observation Summary

Epoch (UT)	$t_{\text{exp}}$ (s)	$n_{\text{dither}}^{\text{a}}$	Sky Level (DN s $^{-1}$ )	Nominal PA (deg)	$\Delta\text{PA}^{\text{b}}$ (deg)	Scale (mas pixel $^{-1}$ )	$x_0^{\text{c}}$ pixels	$y_0^{\text{c}}$ pixels
1996 Oct 6	4800	4	0.006	129.38	0.012(2)	45.5936(8)	408.004(5)	428.143(5)
1999 Mar 30	7200	8	0.006	−51.75	0.0212(7)	45.6028(5)	429.221(3)	437.824(3)
1999 Sep 16 <sup>d</sup>	5191	4	0.005	124.97	0	45.5938	417.948	436.803

<sup>a</sup>The dither pattern was in sets of four images, with  $(\Delta x, \Delta y) = (0,0)$ ,  $(0,0)$ ,  $(5.5, 5.5)$ , and  $(5.5, 5.5)$  pixels.

<sup>b</sup>Defined as the difference between the fitted position angle and the nominal position angle (from the image header and Table 1).

<sup>c</sup> $x$  and  $y$  pixel offsets used for transformation.

<sup>d</sup>The values for this epoch were assumed to be correct.

Note. — See Eqn. 2 for the sense of the transformation.

Table 2. Reference Sources for Astrometry

ID <sup>a</sup>	$\alpha^b - 18^{\text{h}}56^{\text{m}}$ (s)	$\delta^b + 37^{\circ}54'$ (arcsec)	$M_{\text{F606W}}$ (mag)	$\Delta\alpha^c$ (arcsec)	$\Delta\delta^c$ (arcsec)	$\mu_\alpha$ (mas yr <sup>-1</sup> )	$\mu_\delta$ (mas yr <sup>-1</sup> )
100	34.28	29.3	25.0	-12.9651(9)	2.4976(9)	0.1(5)	5.6(6)
102	34.60	21.7	24.5	-9.1416(8)	10.0946(9)	-5.6(3)	-6.6(3)
103	34.85	16.3	23.9	-6.2193(4)	15.4760(3)	-2.7(2)	1.9(2)
104 <sup>d</sup>	34.96	15.6	25.2	-4.924(1)	16.117(1)	0	0
105	35.49	20.6	26.0	1.3560(2)	11.1550(2)	-1.3(7)	-0.9(7)
106	35.56	24.6	22.4	2.2431(3)	7.1809(3)	-2.7(3)	0.9(3)
107	34.50	42.3	23.7	-10.3348(4)	-10.5884(4)	-1.8(3)	-1.2(3)
108 <sup>e</sup>	35.83	46.5	25.0	...	...	...	...
110	36.04	46.0	25.1	8.0253(7)	-14.2280(7)	-0.9(4)	2.4(4)
111	37.07	28.8	24.6	20.1264(4)	2.9624(5)	1.5(3)	4.8(3)
112	36.37	23.9	23.6	11.8772(5)	7.9134(5)	-2.4(2)	-1.0(2)
113	36.12	33.2	23.8	8.8837(3)	-1.411(1)	0.1(9)	6(1)
114	35.93	30.4	24.2	6.6715(4)	1.3405(4)	-0.3(5)	4.8(4)
116	33.70	35.5	24.0	-19.7242(6)	-3.7665(6)	-0.9(3)	-3.3(3)
117 <sup>e</sup>	34.57	22.4	25.8	...	...	...	...
118	34.96	25.2	24.6	-4.8365(6)	6.5790(6)	-1.9(3)	-4.9(3)
119 <sup>e</sup>	35.68	23.6	25.7	...	...	...	...
127	35.36	48.5	26.3	-0.0430(1)	-16.758(1)	-1(1)	1.1(9)
128	35.27	47.2	24.9	-1.1148(9)	-15.45289	-1.2(5)	-1.2(5)
129	35.08	43.5	26.3	-3.3735(3)	-11.782(2)	4.5(8)	1.8(9)
133	35.31	28.7	21.0	-0.6627(4)	3.0372(4)	-0.4(2)	-0.3(2)
201	36.44	21.2	20.4	12.6471(3)	10.6446(3)	-0.7(2)	0.6(2)
202	36.51	31.4	22.0	13.4631(2)	0.4201(2)	0.2(3)	-2.6(3)
19	34.22	39.4	21.9	-13.6277(4)	-7.6757(4)	2.4(2)	2.4(2)
20 <sup>d</sup>	35.05	38.3	23.7	-3.8055(8)	-6.5591(8)	0	0
21	34.80	36.5	21.0	-6.6871(4)	-4.7115(4)	3.9(2)	-2.3(2)
23	35.19	35.4	23.8	-2.0685(5)	-3.6799(5)	-5.0(3)	-6.1(2)
26	36.84	29.0	21.5	17.3585(4)	2.8446(5)	2.2(2)	-11.1(3)
28	34.88	28.9	21.7	-5.7783(5)	2.8325(5)	-0.4(2)	-2.3(2)
X <sup>f</sup>	35.58	36.2	26.1	2.643(2)	-4.504(2)	...	...

<sup>a</sup>ID's are as in W01 where possible; sources 201 and 202 were not present in W01; X is RX J1856.5–3754.

<sup>b</sup>Positions are measured at equinox J2000, epoch 1999.26.

<sup>c</sup>Fiducial positions at epoch 1999.7, relative to  $(x_0, y_0)$  offsets given in Table 1.

<sup>d</sup>Extended source, probably a galaxy.

<sup>e</sup>Rejected from the analysis due to poor position measurements; see Table 3.

<sup>f</sup>For proper motions, see Table 4.

Table 3. Distortion Corrected  $(x, y)$  Source Positions

ID	Epoch								
	1996 Oct			1999 Mar			1999 Sep		
	<i>x</i>	<i>y</i>	<i>N</i> <sup>a</sup>	<i>x</i>	<i>y</i>	<i>N</i> <sup>a</sup>	<i>x</i>	<i>y</i>	<i>N</i> <sup>a</sup>
	(pixels)	(pixels)		(pixels)	(pixels)		(pixels)	(pixels)	
100	269.63(3)	173.83(2)	3	562.43(2)	694.92(2)	8	304.53(2)	170.38(2)	4
102	452.45(1)	132.70(1)	4	379.55(3)	732.33(1)	8	489.55(2)	146.83(1)	4
103	583.81(1)	107.54(1)	4	247.36(2)	755.08(2)	8	623.26(1)	134.02(1)	4
104	612.51(3)	120.50(5)	4	218.50(5)	741.63(7)	8	650.93(5)	149.61(5)	4
105	616.08(4)	295.90(4)	4	218.82(4)	565.99(4)	8	637.53(4)	324.77(4)	3
106	561.03(2)	366.40(2)	4	275.145(9)	496.71(1)	8	576.066(8)	389.601(8)	4
107	84.80(2)	400.36(2)	4	751.80(2)	471.926(9)	8	98.673(9)	378.58(1)	4
108	233.92(33)	725.84(11)	4	609.04(8)	144.08(9)	7	216.36(12)	716.08(11)	4
110	278.43(2)	762.35(2)	4	565.18(2)	106.41(2)	8	257.51(2)	757.17(2)	4
111	738.04(1)	728.20(2)	4	104.91(1)	131.54(1)	8	718.50(2)	766.57(1)	4
112	707.599(9)	519.420(9)	4	131.642(9)	340.811(9)	8	707.46(2)	555.82(2)	4
113	507.48(7)	598.59(2)	4	332.92(2)	265.71(3)	8	501.25(3)	615.74(5)	3
114	523.36(2)	522.78(3)	4	315.58(1)	341.14(1)	8	524.10(1)	541.72(2)	3
116	69.84(2)	146.13(1)	4	761.95(2)	726.29(1)	8	107.72(1)	124.24(2)	1
117	434.37(1)	135.98(1)	4	397.66(3)	729.44(2)	8	471.62(30)	147.99(30)	3
118	452.54(1)	254.49(2)	4	381.66(2)	610.43(2)	8	478.38(1)	268.20(2)	3
119	597.78(3)	375.85(4)	4	238.33(3)	486.51(3)	8	612.02(10)	402.70(13)	3
127	123.33(4)	660.75(6)	4	718.28(4)	210.87(4)	8	112.59(3)	641.37(3)	4
128	130.64(3)	624.33(2)	4	710.32(2)	247.15(2)	7	123.17(2)	605.92(2)	3
129	161.07(4)	534.78(3)	4	677.93(7)	335.92(3)	8	162.31(6)	519.85(5)	4
133	450.297(9)	374.648(8)	4	385.946(8)	490.481(8)	8	465.10(1)	387.523(8)	4
201	764.454(8)	494.44(2)	4	74.173(8)	364.652(8)	8	766.54(1)	536.370(8)	4
202	602.610(8)	650.40(2)	4	239.092(8)	211.774(8)	8	590.571(8)	676.538(8)	4
19	88.005(8)	303.943(9)	4	746.47(2)	568.192(8)	8	111.311(9)	282.994(8)	4
20	243.62(4)	455.03(3)	4	593.76(3)	414.32(3)	8	252.08(4)	447.98(2)	4
21	235.02(1)	380.065(9)	4	601.15(1)	488.972(9)	8	250.279(9)	372.88(1)	4
23	317.345(9)	444.296(9)	4	520.60(2)	423.45(1)	8	325.671(9)	444.27(3)	4
26	698.28(2)	682.24(1)	4	144.40(1)	177.714(8)	8	682.42(1)	717.680(8)	4
28	375.731(8)	290.699(8)	4	458.94(1)	575.797(9)	8	398.67(2)	297.003(8)	4
X	357.93(4)	516.84(4)	4	472.30(4)	333.92(4)	8	368.42(4)	540.08(4)	4

<sup>a</sup>The number of independent measurements used to determine the mean position; see Section 2.1.

Table 4. Motion of RX J1856.5–3754

Parameter	Best-fit Values
$\alpha^a$	$2.6435 \pm 0.0042$
$\delta^a$	$-4.5050 \pm 0.0030$
$\mu_\alpha$ (mas yr $^{-1}$ )	$328 \pm 1$
$\mu_\delta$ (mas yr $^{-1}$ )	$-58 \pm 1$
$\pi$ (mas)	$7 \pm 2$
$D$ (pc)	$140 \pm 40$
$\mu$ (mas yr $^{-1}$ )	$333 \pm 1$
PA (deg)	$100.2 \pm 0.2$
$V_\perp$ (km s $^{-1}$ )	$220 \pm 60$

<sup>a</sup>Fiducial positions at epoch 1999.7, relative to  $(x_0, y_0)$  offsets given in Table 1.

Note. — Best-fit values for  $\mu_\alpha$ ,  $\mu_\delta$ ,  $\pi$  are determined directly from a linear least-squares solution, and errors are  $1-\sigma/68\%$  confidence. Best-fit values and errors for the other parameters are derived from those for  $\mu_\alpha$ ,  $\mu_\delta$  and  $\pi$ .

Table 5. Implied Distances to Neutron Stars

Name	kT (eV)	<i>V</i> (mag)	$d_{100}$	Refs.
RX J1856.5-3754	57	25.7	1.4	1,2, this work
RX J0720.4-3125	79	26.6 <sup>a</sup>	3.0	3,4
RX J1308.8+2127	118	28.3	6.7	5,6
PSR B0656+14 <sup>b</sup>	73	27.3	3.3	7,8,9

References. — 1 — Pons et al. 2001; 2 — van Kerkwijk & Kulkarni 2001; 3 — Haberl et al. 1997; 4 — Kulkarni & van Kerkwijk 1998; 5 — Schweppe et al. 1999; 6 — Kaplan et al. 2001, in preparation; 7 — Pavlov, Welty, & Córdova 1997; 8 — Koptsevich et al. 2001; 9 — Zavlin et al. 2001, in preparation

<sup>a</sup>*B* magnitude.

<sup>b</sup>We have taken the temperature of the dominant black-body component, and extrapolated the *V* magnitude from the Rayleigh-Jeans tail found in the UV.

Note. — Calibrated using the parallax of RX J1856.5-3754; see Section 3, Eqn. 3.